

## **Localized Depth of Galvanic Corrosion at Dissimilar Metal Welding**

### **A508/Inconel 182/316L**

**DOI : 10.36909/jer.18721**

Chaur-Jeng Wang, Prihatno Kusdiyarto\*, Chen-Yu Chen

*Department of Mechanical Engineering, National Taiwan University of Science and Technology, No.43, Keelung Rd., Sec.4, Da'an Dist., Taipei City 10607, Taiwan.*

*\* Corresponding author: D10703818@mail.ntust.edu.tw ; prihatnokusdiyarto@uny.ac.id*

#### **ABSTRACT**

Recently, efforts have been made to develop the use of dissimilar metal welding in industrial components. Pressurized water reactors (PWR) in nuclear power plants frequently use dissimilar metal welding (DMW) in their primary water systems (NPP). The selection of the combination of stainless steel and low alloy steel is adjusted to the working conditions of work in high-temperature environments. Nickel-based Inconel 82/182 alloy is used as a weld filler in the GTAW method of joining to produce A508/Inconel-182/316L dissimilar welds with variations in the immersion time of the material at high temperatures. The depth of galvanic corrosion related to morphology using an optical microscope and SEM, changes in potential and current density using a potentiodynamic polarization test, and depth of galvanic corrosion using surface profiler ( $\alpha$ -step) were thoroughly investigated. The results showed that low alloy steel A508 generally suffered from corrosion attacks. Still, the most severe corrosion attack was in the weld joint interface area of low alloy steel A508/Inconel 182 due to the influence of galvanic corrosion. These symptoms will not be seen if observed on the outside of the surface only, but severe symptoms occur on the inside of the weld joint A508/Inconel 182. Finally, there has been a change in the shape of the gap and concave (depth of galvanic corrosion effect) of the welded joint interface between Inconel 182 and low alloy steel

A508 because the effects of galvanic corrosion with changes in potential, current density, and immersion time of dissimilar welded materials.

**Keywords:** Corrosion depth, dissimilar metal welding, galvanic corrosion, low alloy steel A508, and stainless steel 316L.

## INTRODUCTION

Various steel auxiliary devices are commonly required for industrial applications and material corrosion is a widespread phenomenon(Ahmed et al., 2021; Lieth et al., 2021). In a dissimilar metal welded (DMW) nuclear power plant, the local depth of galvanic corrosion and microstructures were investigated(Wang et al., 2012). Ferritic steel pipe nozzles from pressure vessels must be joined to wells of austenitic stainless-steel pipe for improved weldability to protect the nozzle end pipes from serious corrosion risks(Wang et al., 2013). Recently, nuclear power plants used application equipment and high-temperature water pipes, which use stainless steel 316L to be the solution of choice(Du et al., 2016; Zhu et al., 2016). Various techniques and efforts continue to be developed regarding the study of combining dissimilar steel materials, especially for integral components of nuclear power plants (NPP) such as reactor pressure, nozzle pipes, offshore wells, and hot steam inner wall pipes in incinerators(Liang et al., 2021; Liu et al., 2021). The reactor pressure vessel and the pressurized water reactor nozzle are usually made of low alloy steel (LAS)(Choi et al., 2019; Fatima et al., 2021; Kim et al., 2015).

Galvanic methods have primarily been used in the study of uniform corrosion, especially in low alloy steel A508 and Inconel 182 (IN182) weldment HAZ (Heat Affected Zone) areas. The weld filler metal used Inconel 182 (Ni-based metals) to connect low alloy steel to Ni-based or austenitic stainless-steel materials since Ni-based weld filler metals have higher coefficients of thermal (Jang et al., 2008; Wang et al., 2015). On the inner oxide film occurred spinel oxide and Cr<sub>2</sub>O<sub>3</sub> precipitations on the Inconel 182/316L side(Choi et al., 2019;

Wang et al., 2017). Furthermore, the metals that are contaminated with chlorine when in contact with steel will corrode low alloy steel (LAS) and have a high probability of increasing galvanic corrosion (Okonkwo et al., 2021). Thus, research shows that stainless steels will be passive to low alloy steels, so the risk of galvanic corrosion on carbon steels reduces significantly over time (X.G. Feng, 2016). Previous studies(Okonkwo et al., 2019) found that in the welded parts of A508 and other series stainless steel areas, the fine-grained region of low-alloy steel near the fusion boundary is the most prone to galvanic corrosion. However, the crack produced by galvanic corrosion may induce crevice corrosion, which intensifies the corrosion of welded parts(Park et al., 2021).

At present, the significant gap in research is in the occurrence of galvanic effects in the area of local corrosion depth on the inside of the A508/Inconel 182 connection interface on the A508/Inconel 182/316L dissimilar weldment, where this phenomenon is not clearly visible if only seen from the outer surface of the weld joint. In particular, the effect of immersion time on galvanic corrosion was investigated using electrochemical polarization potentiodynamic methods, energy dispersive spectroscopy (EDS) technique, scanning electron microscope (SEM) testing, and surface profiler ( $\alpha$ -step) testing to measure the depth after corrosion experiments.

## METHODS

### *MATERIAL COMPONENT*

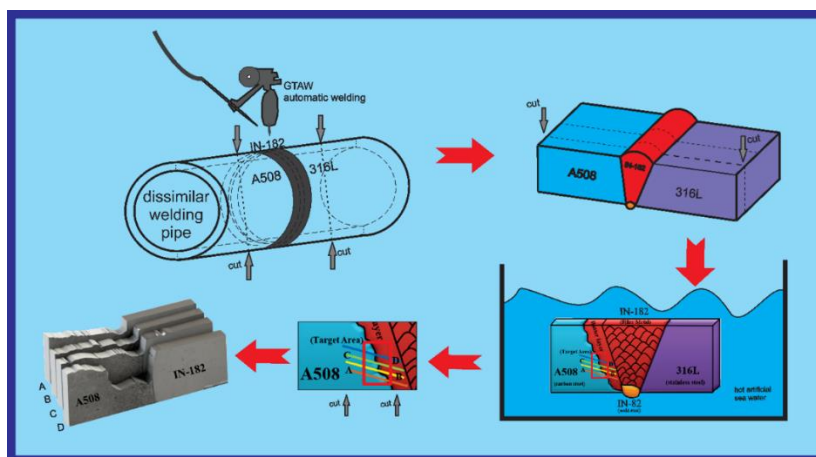


Figure 1: A508/Inconel182/316L dissimilar welding specimen to determine and observe the

gap depth caused by galvanic corrosion with various immersion times.

The materials used in this work for dissimilar weldment are A508 and 316L plates. The butter layer and filler layer of dissimilar butt joints use nickel-based Inconel 182 alloys (ERNiCrFe-3), and the bottom butt joint/ root joint uses nickel-based Inconel 82 Alloy (ERNiCr-3). The A508/Inconel 182/316L dissimilar welding piece is used as the electrochemical test piece. Therefore, the dissimilar metal welding (DMW), which was welded using the gas tungsten arc welding (GTAW) method using an automatic wire feeder carried out on A508 low alloy steel automatically controlled with 316L stainless steel carried out by the cladding process (Sabzi et al., 2021). In Figure 1, the specimens were cut in vertical and cross-section directions by a wire electrical discharging machine (WEDM). The specimens were ground and polished with 1500 grit size sandpaper, then polished with  $Al_2O_3$ , after which they were degreased and dried with an ethanol ultrasonic wave. Finally, they were washed with deionized water, and after being cleaned, they were put in a dry box.

### PROCESS

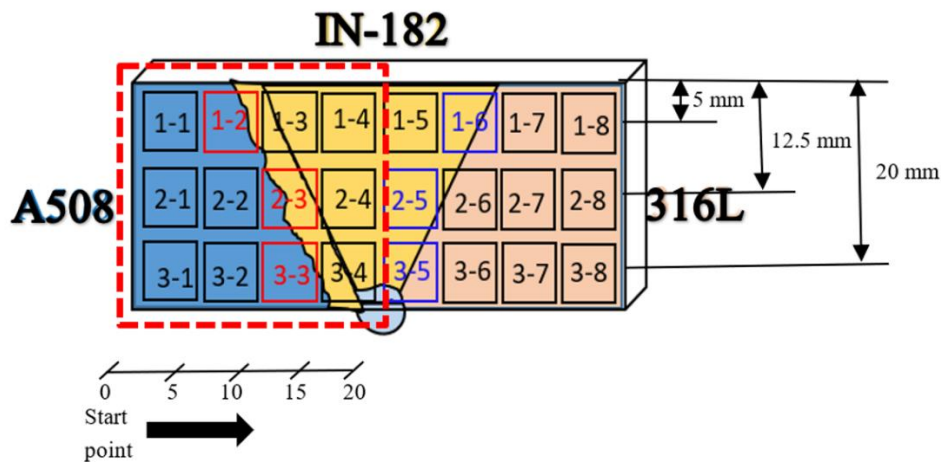


Figure 2: The test area of  $0.25 \text{ cm}^2$  for local potentiodynamic polarization.

The electrochemical experiments used three electrodes in the process with potentiodynamic polarization testing. Namely, the reference electrode was a saturated calomel electrode (SCE), the auxiliary electrode was a platinum electrode, and the working electrode was a sample. All

potentials in the standard were based on the SCE potential. The first time, the experiments were placed in a water bath at 25°C, and the samples were immersed in sodium chloride solution for 7200 seconds until the open circuit potential (OCP) was significantly stabilized. The second time, pure N<sub>2</sub> is added into the solution and inflated for 1800 seconds, and then the coupon is put in the reaction glass; the solution is deoxidized for another 7200 seconds. The final time, the potentiodynamic polarization scan started at -1500 until 1000 mV with a scan rate of 5 mV/s.

The immersion test piece is taken from different positions of the sample. In accordance with the ASTM G31 specifications, the size of the test piece is set at 50 mm in length, 25 mm in width, and  $4.85 \pm 0.05$  mm in thickness. Metallurgical observations were carried out using the Olympus BX41M series metallurgical microscope to analyze the symptoms that occur in the HAZ area material and the dissimilar welding joints. Using SEM analysis (JOEL JSM-6390LV), the overall morphology of the weldment is known. The local corrosion resistance was analyzed by the potentiodynamic polarization method of the constant potential meter (GAMRY G750) as seen in Figure 2. After the immersion test, the depth of the galvanic corrosion test piece was measured with a surface profiler ( $\alpha$ -step) to find out the depth of the galvanic corrosion effect in the cross-section area.

## RESULT AND DISCUSSION

### *MICROSTRUCTURES OF DISSIMILAR METAL WELDING (DMW)*

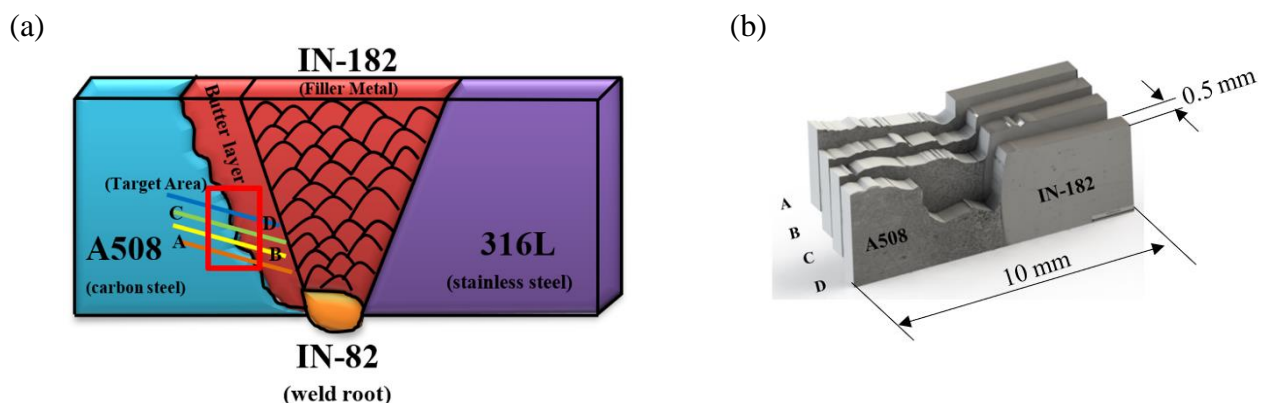


Figure 3: (a) Metallographic diagram cross-sectional gap at interface A508 /Inconel 182 in A, B, C, and D lines. (b) The cross-section material area (red square) after got immersion testing for three months.

In the visual inspection shown in Figure 3a, two different metals were connected and immersed in an electrolyte solution and formed galvanic cells. Corrosion attacks at the junction between the two different alloys were limited to only one of the two steel sheets combined with stainless steel, causing galvanic corrosion. The specimens were cut in vertical and cross-section directions by a wire electrical discharging machine (WEDM). Four cutting samples were taken A, B, C and D lines in the area indicated by corrosion, namely the red box in Fig.3a. While Fig. 3b is an image of the result of an optical microscope in three-dimensional form from the results of pieces of samples A, B, C, and D lines. In the observation of Figure 3b by testing optical microscope equipment, it is explained that there is a phenomenon of massive grinding of carbon steel material on the inside of different types of welded joints. Figure 3c observations using an optical microscope, and it is found that there is a significant gap in the connection between carbon steel and Inconel 182 with increasing artificial seawater immersion time. Therefore, limiting the anode attack rate to an area sufficiently close to the junction between the different alloys requires resistance to the electrolyte. Nevertheless, in the case of two different alloys being combined, the more negative or active  $E_{corr}$  having excess electron activity will then be lost to the more positive alloy. Hence, galvanic corrosion will attack the most active (negative) alloys(Huang et al., 2019).



Figure 4. Observe the macroscopic surface of the A508/IN-182/316L specimen after immersion

In Figure 4, the HAZ area of the A508 low alloy steel on the left of the sample was the area that was affected by galvanic corrosion, while the weld metal area of Inconel 182 was not significantly affected by corrosion, and the non-corroded area was the reference area used for corrosion area. After one, two, and three months of alternating observations in the acidic environment, a topographic analysis was performed using optical microscope equipment for sample observation.

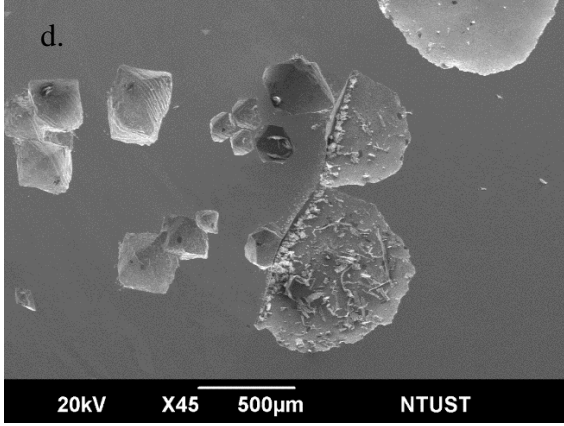
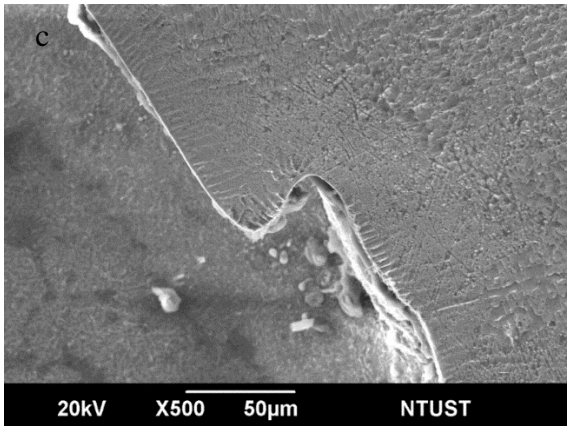
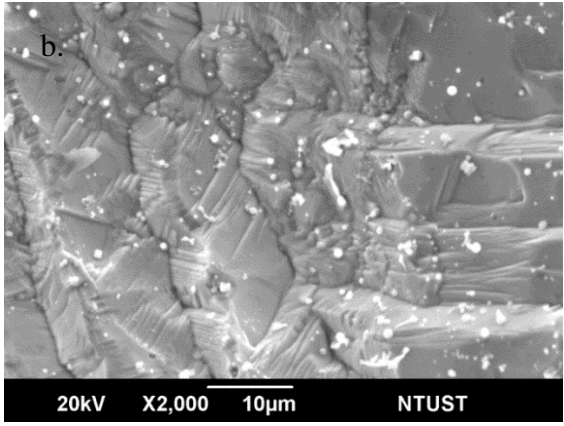
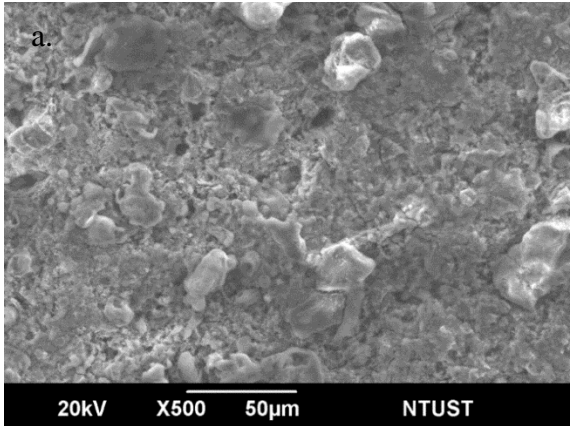


Figure 5: The morphology of the corroded area is shown by the SEM result of the nickel-based Inconel 182 and steel A508, which indicates that there is apparent galvanic corrosion. (a) A508 base material (b) Inconel 182 base material (c) A508 and Inconel 182 weld joint (d) typical pitting morphology of Inconel 182 and 316Lweld joint.

Based on Figure 5 shows the SEM pictures of 316L stainless steel and low alloy steel A508 after galvanic corrosion at 25°C in a 3.5% NaCl solution. It can be seen from Figure 5 that after galvanic corrosion, the surface of low alloy steel was damaged and porous, and material distribution was unequal. Consequently, as the concentration of the corrosive solution increased, corrosion products appeared on the surface of the material.

Therefore, as seen in Figure 5, most of the galvanic corrosion products of low alloy steel were clusters of material structures, and an increase in the concentration of the solution and duration of immersion caused the diameter and volume of the oxide particles to increase. In comparison, the surface of 316L stainless steel had a uniform structure and thick corrosion, and the oxidation products were often lattice structures of different lengths. The base metal of A508 was an area that did not receive heat distribution, so the structural form was relatively the same, where the austenite was shown in the bright white part while the ferrite was shown in the darker part. The macroscopic surface of the A508/Inconel 182 test piece was observed after immersion and left uncleaned. The surface of A508 metal was covered with black products. After cleaning, the microscopic surface of A508 showed an off-white substrate, and there was no apparent corrosion on the surface of Inconel 182. The anode metal (A508) closer to the cathode metal (Inconel 182) in the weldment will generate a larger corrosion current and corrosion depth due to the distance effect. Therefore, when the A508/Inconel 182 test piece is immersed for two months, and the test piece is immersed for three months at the junction of A508 and Inconel 182, there are apparent slits caused by corrosion on the A508 side. The black product after the immersion test appeared in the base material area of the A508 low-alloy steel of the test piece

after the analysis was indicated as the composition of the  $\text{Fe}_3\text{O}_4$  material. This cluster resembles a neatly arranged chain structure caused by magnetic interactions between particles, and also the morphology is smaller than 20 nm resembling a ball shape and black in color. Its oxide layer is insoluble in water, alkali, and ethanol solutions. It can protect the A508 substrate and reduce corrosion. The Inconel 182 and 316L contain more chromium elements and produce a  $\text{Cr}_2\text{O}_3$  protective layer, so it was resistant to corrosion attack, compared with A508 low-alloy steel.

#### THE EFFECT OF POTENTIAL, GALVANIC CURRENT, AND GALVANIC CORROSION DEPTH.

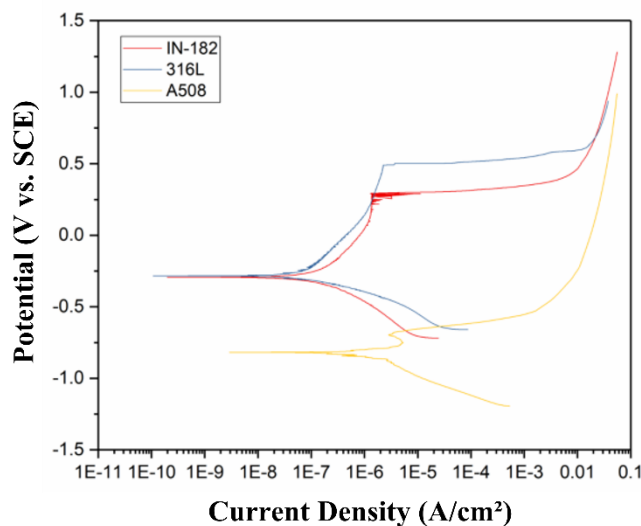


Figure 6: Potential polarization curve of dissimilar weldment materials for weldment base 316L, Inconel 182, and A508.

The results of avoiding gaps and measuring the depth of A508/Inconel 182/316L, as shown in Figure 6, depict monthly data on the corrosion depth of the specimen's upper, middle, and lower measurement lines. There is no difference in depth loss between the Inconel 182 and the 316L. When the depth of corrosion from Inconel 182 to A508 began to diminish, there was deeper corrosion at the A508/Inconel 182 contact point and the interface between the heat-affected zone and the base material. However, the solution resistance grows with distance, preventing galvanic corrosion and finally transforming into general uniform corrosion, with the depth of corrosion slowing down. From one month to three months, the average uniform

corrosion depth of A508 is approximately 69.33  $\mu\text{m}$ , 91.92  $\mu\text{m}$ , 98.33  $\mu\text{m}$ , and the corrosion loss per month is around 69.33 mg, 22.59 mg, 6.41 mg. Figure 6 depicts the corrosion loss trend. The results reveal that the uniform corrosion rate of base metal A508 slows down with time in a long-term immersion test.

Table 1: The data of 0.25  $\text{cm}^2$  local area of potentiodynamic polarization of A508/ Inconel 182.

|   | Layer 1 |       |       |       | Layer 2 |       |       |       | Layer 3 |       |       |       |
|---|---------|-------|-------|-------|---------|-------|-------|-------|---------|-------|-------|-------|
|   | 1-1     | 1-2   | 1-3   | 1-4   | 2-1     | 2-2   | 2-3   | 2-4   | 3-1     | 3-2   | 3-3   | 3-4   |
| $I_{corr}$<br>( $\text{nA}/\text{cm}^2$ ) | 457     | 298   | 59.4  | 54.1  | 124     | 176   | 382   | 25.4  | 491     | 293   | 161   | 19.7  |
| $E_{corr}$<br>(V vs. SCE)                 | -0.82   | -0.84 | -0.31 | -0.38 | -0.85   | -0.85 | -0.51 | -0.30 | -0.86   | -0.87 | -0.88 | -0.31 |
| CR (mpy)                                  | 0.209   | 0.136 | 0.027 | 0.024 | 0.056   | 0.080 | 0.175 | 0.011 | 0.225   | 0.134 | 0.073 | 0.008 |

Based on Table 1, it can be explained that in layer 1, from the direction of low alloy steel 508 to the direction of Inconel 182,  $I_{corr}$  moves lower, and  $E_{corr}$  -0.84 (V vs. SCE) is a large value whose position is in a different type of connection compared to other  $E_{corr}$  in the first row of the first layer. In layer 2,  $I_{corr}$  reaches the largest value of 382  $\text{nA}/\text{cm}^2$  compared to the second row of layer 1, and the  $E_{corr}$  condition in layer 2 decreases towards Inconel 182. Finally, in layer 3,  $I_{corr}$  decreased, and  $E_{corr}$  -0.88 (V vs. SCE) had the largest value among others in one line of layer 3. This can be illustrated in the weld joint area A508/ Inconel 182 that the condition of layer 1,  $I_{corr}$  298  $\text{nA}/\text{cm}^2$  and  $E_{corr}$  -0.84 (V vs. SCE), and in layer 2,  $I_{corr}$  382  $\text{nA}/\text{cm}^2$  and  $E_{corr}$  -0.51 (V vs. SCE). Nevertheless, in layer 2,  $I_{corr}$  has increased, and  $E_{corr}$  has decreased compared to the connection conditions in layer 1. Moreover, for the results on layer 3 of the connection,  $I_{corr}$  161  $\text{nA}/\text{cm}^2$  and  $E_{corr}$  -0.88 (V vs. SCE).  $I_{corr}$  decreased, and  $E_{corr}$  increased compared to layer 2.

The electrochemical behavior of local samples of area 2-3 on layer two being welded leads to the positive volt potential of the sample in area 1-2 on layer one and area 3-3 on layer

three, which have a similar volt potential. For the three samples, the corrosion rate increased by 0.175 mpy in layer two areas 2-3 where morphological test samples were taken. This indicates that the influence of the immersion time and galvanic corrosion of various types of connection materials is related to the small variation in the corrosion rate as well as the potential for corrosion that was observed. After that, more polarization experiments are performed on the sample to determine the metallurgical characterization technique(Adam Khan et al., 2020).

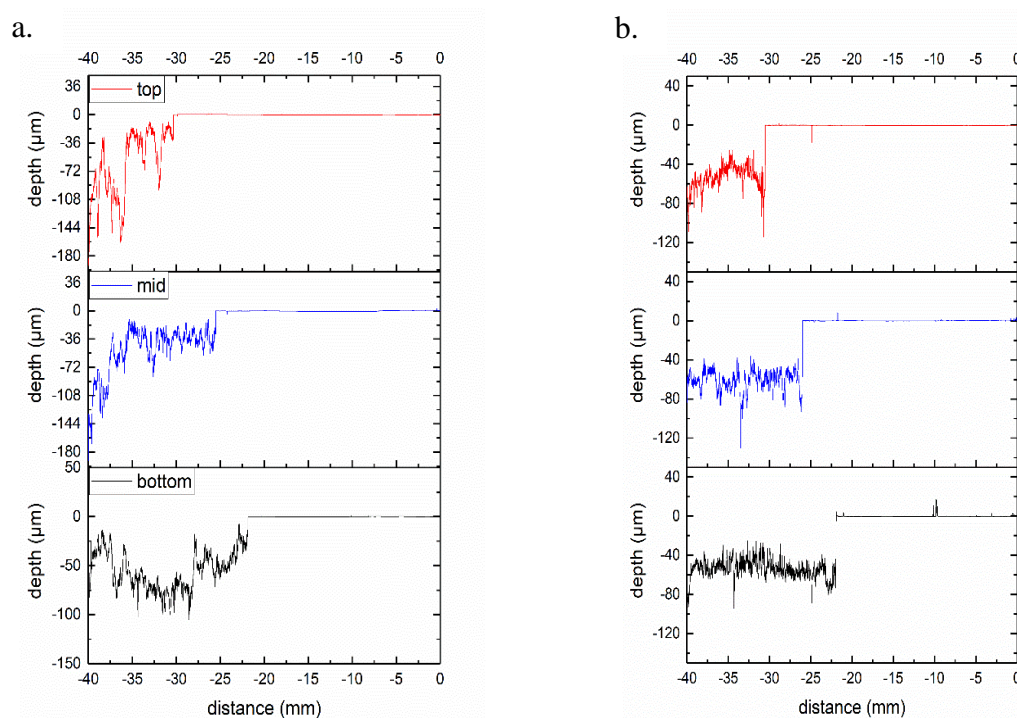


Figure 7: The amount of thinning of the test piece of A508/Inconel 182/316L. a) Three months A508/ Inconel 182/316L front side. b) Three months A508/Inconel 182/316L back side.

Based on Figure 7, the specimens measured by  $\alpha$ -step, the depth of corrosion in this area is very small for immersion one month and two month. In this case, it is found that the area of 2-3 weld metal immersion, for one month, the minimum corrosion depth is 17.9  $\mu\text{m}$  and becomes 22.0  $\mu\text{m}$  after immersion for two months and in the third month is 63  $\mu\text{m}$ . Also, the maximum corrosion depth from one month to three months is 149  $\mu\text{m}$ , 220  $\mu\text{m}$ , and 208  $\mu\text{m}$ , respectively. The sampling position is not necessarily the maximum depth but the average corrosion depth for reference only. In addition, the tendency for galvanic corrosion is slowed

down by the highly corroded heterogeneous interface perpendicular to the direction of the base material. Therefore, the average depth of corrosion in each area immersed for one and two months shows a uniform corrosion pattern. In addition, a small galvanic corrosion phenomenon occurred, but in the third month, a more serious galvanic corrosion occurred. Finally, with the increases in corrosion current density in the electrochemical test, the average corrosion depth also increases.

### **CONCLUSIONS**

In this study, the observation of the depth of galvanic corrosion on the A508/Inconel 182/316L dissimilar welding material mainly focuses on the A508/Inconel 182 area. Rather on the inside of the A508/Inconel 182 interface joint, there was severe damage and strong corrosion because of galvanic corrosion. It can be concluded that:

- The maximum corrosion depths from one month to three months of testing are 149  $\mu\text{m}$ , 220  $\mu\text{m}$ , and 208  $\mu\text{m}$ . In the third month, there was more serious galvanic corrosion. With the increase in the corrosion current density in the electrochemical test, the average corrosion depth also increases.
- The anode metal, in this case, low carbon steel A508, undergoes galvanic corrosion because it is a metal that has a lower potential resulting in an increased corrosion rate. Meanwhile, the corrosion rate of stainless steel 316L significantly decreases because the interfacial potential of the steel was cathodic polarized so that it is close to its immune zone.

### **ACKNOWLEDGMENTS**

The authors are very grateful to the Ministry of Science and Technology of the Republic of China for funding support grant no. 108-NU-E-011-001-NU.



## REFERENCES

- Adam Khan, M., Chellaganesh, D., Uthayakumar, M., Winowlin Jappes, J.T., Duraiselvam, M. 2020. Electrochemical Behaviour and Surface Studies on Austenitic Stainless Steel and Nickel-Based Superalloy Dissimilar Weld Joints. *Journal of Materials Forming, Machining and Tribology*: 251–266.
- Ahmed, M.M.Z., Abdul-Maksoud, M.A.A., Seleman, M.M.E.-S. 2021. Effect of dwelling time and plunge depth on the joint properties of the dissimilar friction stir spot welded aluminum and steel. *Journal of Engineering Research* 9.
- Choi, K.J., Yoo, S.C., Kim, S., Kim, T., Ham, J., Lee, J., Kim, J.H. 2019. Microstructural evolution and corrosion behaviour of thermally aged dissimilar metal welds of low-alloy steel and nickel-based alloy. *Corros Sci* 153: 138–149.
- Du, D., Chen, K., Lu, H., Zhang, L., Shi, X., Xu, X., Andresen, P.L. 2016. Effects of chloride and oxygen on stress corrosion cracking of cold worked 316/316L austenitic stainless steel in high temperature water. *Corros Sci* 110: 134–142.
- Fatima, A., Wasif, M., Mumtaz, M.O. 2021. Optimization of process parameters in turning of nuclear graded steel alloy (AISI-410) for sustainable manufacture. *Journal of Engineering Research* 9.
- Huang, C., Huang, F., Liu, H.-X., Hu, Q., Liu, J. 2019. The galvanic effect of high-strength weathering steel welded joints and its influence on corrosion resistance. *Corrosion Engineering, Science and Technology* 54: 556–566.
- Jang, C., Lee, J., Sung Kim, J., Eun Jin, T. 2008. Mechanical property variation within Inconel 82/182 dissimilar metal weld between low alloy steel and 316 stainless steel. *International Journal of Pressure Vessels and Piping* 85: 635–646.
- Kim, M.-C., Park, S.-G., Lee, K.-H., Lee, B.-S. 2015. Comparison of fracture properties in SA508 Gr.3 and Gr.4N high strength low alloy steels for advanced pressure vessel

- materials. *International Journal of Pressure Vessels and Piping* 131: 60–66.
- Liang, H., Duan, Y., Wu, M., Liu, Y., Lin, T. 2021. Relationship between perforation depth and core flow efficiency. *Journal of Engineering Research*.
- Lieth, H.M., Al-Sabur, R., Jassim, R.J., Alsahlani, A. 2021. Enhancement of corrosion resistance and mechanical properties of API 5L X60 steel by heat treatments in different environments. *Journal of Engineering Research*.
- Liu, D.-G., Yang, T.-T., Liu, Y.-L., Luo, L.-M., Wu, Y.-C. 2021. Thermal shock and tritium resistance of SiO<sub>2</sub> coating on the inner wall of 316L stainless steel pipeline. *Vacuum* 185 (110032).
- Okonkwo, B.O., Ming, H., Wang, J., Han, E.-H., Rahimi, E., Davoodi, A., Hosseinpour, S. 2021. A new method to determine the synergistic effects of area ratio and microstructure on the galvanic corrosion of LAS A508/309 L/308 L S.S. dissimilar metals weld. *J Mater Sci Technol* 78: 38–50.
- Okonkwo, B.O., Ming, H., Zhang, Z., Wang, J., Rahimi, E., Hosseinpour, S., Davoodi, A. 2019. Microscale investigation of the correlation between microstructure and galvanic corrosion of low alloy steel A508 and its welded 309/308L stainless steel overlayer. *Corros Sci* 154: 49–60.
- Park, J.S., Lee, J.W., Kim, S.J. 2021. Hydrogen-Induced Cracking Caused by Galvanic Corrosion of Steel Weld in a Sour Environment. *Materials* 14: 5282.
- Sabzi, M., Mousavi Anijdan, S.H., Eivani, A.R., Park, N., Jafarian, H.R. 2021. The effect of pulse current changes in PCGTAW on microstructural evolution, drastic improvement in mechanical properties, and fracture mode of dissimilar welded joint of AISI 316L-AISI 310S stainless steels. *Materials Science and Engineering: A* 823 (141700).
- Wang, H.T., Wang, G.Z., Xuan, F.Z., Liu, C.J., Tu, S.T. 2012. Local Mechanical Properties and Microstructures of Alloy52M Dissimilar Metal Welded Joint between A508 Ferritic

Steel and 316L Stainless Steel. *Adv Mat Res* 509: 103–110.

Wang, H.T., Wang, G.Z., Xuan, F.Z., Liu, C.J., Tu, S.T. 2013. Local mechanical properties of a dissimilar metal welded joint in nuclear powersystems. *Materials Science and Engineering. A* 568: 108–117.

Wang, W., Cao, X., Lu, Y., Ding, X., Shoji, T. 2017. TEM study on oxide mechanism of the dissimilar welds between 316 stainless steels/Inconel 182 in high temperature and high pressure water. *Mater Charact* 131: 339–347.

Wang, W., Lu, Y., Ding, X., Shoji, T. 2015. Microstructures and microhardness at fusion boundary of 316 stainless steel/Inconel 182 dissimilar welding. *Mater Charact* 107: 255–261.

X.G. Feng, J.Q.L.C.H.Z.C.L.Y.K.J.Y.W.X.D.C. 2016. Galvanic Corrosion Between AISI304 Stainless Steel and Carbon Steel in Chloride Contaminated Mortars. *Int J Electrochem Sci*: 5226–5233.

Zhu, R., Wang, J., Zhang, L., Zhang, Z., Han, E. 2016. Stress corrosion cracking of 316L HAZ for 316L stainless steel/Inconel 52M dissimilar metal weld joint in simulated primary water. *Corros Sci* 112: 373–384.